

TURBULENCE STRUCTURE DOWNSTREAM OF A LINEAR COMPRESSOR CASCADE

T. O. Jelly

Department of Engineering
Whittle Laboratory, University of Cambridge
CB3 0DY, United Kingdom
toj23@cam.ac.uk

L. Di Mare

Department of Mechanical Engineering
Imperial College London
SW7 2AZ, United Kingdom
l.di.mare@imperial.ac.uk

I. J. Day

Department of Engineering
Whittle Laboratory, University of Cambridge
CB3 0DY, United Kingdom
ijd1000@cam.ac.uk

ABSTRACT

Single- and two-point hot-wire measurements have been acquired in the near-wake of a linear compressor cascade at a chord Reynolds number of 7.5×10^5 . A measurement technique based on a rotated pair of single straight-wire sensors has been developed in order to examine Reynolds stresses, energy spectra and space-time correlations downstream of the stationary blade row. The current results imply the existence of large-scale, organised structures in the near-wake region and highlight their potential to transport momentum and energy through compressor blade passages. This work represents an initial step towards a detailed characterisation of turbulence structure in compressor annuli and provides a data set that will prove useful for future measurement campaigns, as well as the set up of scaled-resolved computations.

INTRODUCTION

The characterisation of turbulence is possible using a variety of hot-wire anemometry (HWA) techniques. For example, turbulence statistics can be computed directly from the instantaneous response of a triple-wire sensor (Paulsen, 1983) but, relative to double and single-wires, introduce a larger disturbance in to the flow, and require complex calibration and maintenance procedures. If the details of instantaneous velocity components are not imperative, a statistical description of the flow can be obtained using single-wire techniques, provided that the sensor's angular response is known.

By invoking Reynolds' decomposition and applying standard laws of averaging, statistical moments of the instantaneous sensor response equations can be obtained. In addition, by taking single-sensor measurements at two separated points in the flow, the spatio-temporal turbulence structure can be examined by evaluating the correlation function (Townsend, 1976). Furthermore, single- and two-point statistics can be mapped to an inertial frame of reference by solving a system of equations based on measurements acquired at several known sensor orientations.

Rotated single-wire techniques

In the past, rotated single-wire techniques have characterised turbulence in a number of flow configurations. For example, single-sensors have measured the production of mean streamwise vorticity in the corners of non-circular ducts (Brundrett & Baines, 1964) and the distribution of Reynolds shear stress in fully-developed turbulent pipe flow (Fujita & Kovaszny, 1968). Previous experiments have also characterised turbulence in boundary layers with circumferential strain (Bissonnette & Mellor, 1974), strong transverse pressure gradients (De Grande & Kool, 1981), and downstream of a bi-plane grid (Russ & Simon, 1991). Relative to double-component two-wire measurements, single-wire results often show good agreement — provided that turbulence intensities remain less than ten percent.

For flows with turbulence intensities greater than ten percent, it is customary to retain higher order velocity correlations in the response equations. For example, by retaining third-order terms in a power series expansion of the instantaneous effective cooling velocity, Champagne & Sleicher (1967) derived response equations capable of characterising flow with a turbulence intensity of twenty percent. High levels of turbulence intensity are common feature of turbomachinery flow configurations. In the trailing edge region of a highly loaded compressor rotor blade, for example, axial turbulence intensities in excess of fifty percent have been reported (Ravindranath & Lakshminarayana, 1981) and warrant a detailed investigation of turbulence in turbomachinery flow configurations.

Turbulence in compressor configurations

Turbulence is a fundamental factor in the transport of momentum and energy within the annulus of axial compressors and its significance with respect to large scale, organised motion is key to being able to predict performance and stability limits (Evans, 1975). The turbulence structure in compressors was first examined in detail by Lakshminarayana and his co-workers. For example, turbulence in-

tensities, decay rates and energy spectra were obtained in both the near wake (Lakshminarayana & Reynolds, 1980) and far wake (Ravindranath & Lakshminarayana, 1981) of a compressor rotor blade using triple-sensor hot-wire probes.

The significance of three-dimensionality was demonstrated by Adkins & Smith (1982), and later by Galimore & Cumpsty (1986), who highlighted the interplay between secondary motion and relatively small-scale turbulence in multi-stage turbomachines. Turbulence autocorrelation functions were measured by Camp & Shin (1995) and, after invoking Taylor's hypothesis, inferred the presence of structures with integral length scales of up to forty percent blade chord at off-design, near-stall conditions.

In the current work, a compressor blade row is modelled as a linear cascade of airfoils. Relative to a compressor blade row, cascade configurations facilitate rapid development of experimental procedures, measurement techniques and related post-processing routines, in exchange for some slight discrepancies in flow physics (Cumpsty, 1989, p.334). A number of previous experimental campaigns have reported turbulence statistics in cascade configurations using, for example, single-wire sensors (Muthanna & Devenport, 2004), cross-wire sensors (Wenger *et al.*, 2004) and three-component laser Doppler anemometry (Tian *et al.*, 2007) techniques. In general, however, a detailed description of the spatio-temporal structure of turbulence in turbomachinery remains largely unavailable in the literature.

Motivation and objectives

In axial-flow compressor configurations, fully-resolved whole-annulus simulations remain too costly for general use (Denton, 2010). Alternatively, simplified compressor geometries, such as a linear cascade, are amenable to scale-resolving computations that include large-eddy simulation (LES). However, LES often requires the synthesis of turbulent inflow conditions based on single- and two-point statistics which are typically acquired in the laboratory (di Mare *et al.*, 2006). Therefore, suitable experimental techniques must be established before hi-fidelity simulations can be performed.

This study examines the structure and energetics of turbulence downstream of a linear compressor cascade at a chord Reynolds number of 7.5×10^5 . The details of turbulence structure in the near-wake region are vital since the unsteady fluid motions impact the aeroacoustic, aerodynamic and structural properties of the successive blade rows (Lakshminarayana & Reynolds, 1980). Based on a measurement procedure that utilises a pair of rotated single straight-wire sensors, a number of single- and two-point turbulence statistics have been calculated in order to examine the large-scale, orderly motions downstream of the stationary blade row.

METHODOLOGY

This section reports the methodology adopted over the course of the measurement campaign and is divided into three parts. First, a derivation of the hot-wire response equations is provided. Second, descriptions of the wind-tunnel facility and of the linear compressor cascade are given. Finally, details of data acquisition and typical sampling parameters are reported, as well as some additional information regarding data post-processing.

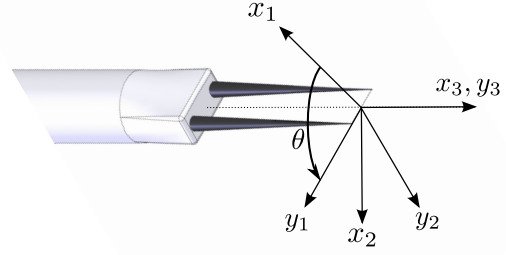


Figure 1. Schematic of straight single-wire sensor. The rotating wire-fixed and inertial coordinate systems are denoted by y_i and x_i , respectively. The angle formed by the wire with the x_1 axis is denoted θ .

Hot-wire response equations

With reference to figure 1, let u_i be the velocity component along the x_i axis. Let the probe be a single straight-wire probe with its stem aligned along the x_3 axis and let θ be the angle formed by the plane containing the prongs and the sensor with the x_1 axis. Then the velocity components v_i in the rotating wire-fixed coordinate system y_i are related by the following

$$\begin{bmatrix} v_1 \\ v_2 \\ v_3 \end{bmatrix} = \begin{bmatrix} \cos \theta & \sin \theta & 0 \\ -\sin \theta & \cos \theta & 0 \\ 0 & 0 & 1 \end{bmatrix} \begin{bmatrix} u_1 \\ u_2 \\ u_3 \end{bmatrix}$$

which can be written compactly as

$$v_i = M_{ij}u_j \quad (1)$$

where M_{ij} is the rotation matrix.

The instantaneous effective cooling velocity, q_e , is described by Jørgensen's equation (Jørgensen, 1971)

$$q_e = \varepsilon^2 d_1^2 v_1^2 + d_2^2 v_2^2 + d_3^2 v_3^2 \quad (2)$$

where d_i represent the wire sensitivity coefficients. Typical values for d_2 and d_3 are 1.0 and 1.05, respectively (Bruun, 1995). The small parameter, ε , in Jørgensen's equation 2 is introduced in order to represent the sensitivity of the wire to the v_1 component (Webster, 1962).

By assuming that the turbulent fluctuations are small, relative to the mean, Reynolds' decomposition for the instantaneous velocity components u_i can be written as

$$u_i = \bar{u}_i + \varepsilon u'_i \quad (3)$$

where \bar{u}_i and u'_i denote time-averaged and stochastic velocity components, respectively.

Substituting Reynolds' decomposition 3 into the right-hand side of Jørgensen's equation 2 yields

$$q_e = G_{hk} \left(\bar{u}_h \bar{u}_k + \varepsilon \bar{u}_h u'_k + \varepsilon \bar{u}_k u'_h + \varepsilon^2 u'_h u'_k \right) \quad (4)$$

where $G_{hk} = \varepsilon^2 d_1^2 M_{1k} M_{1h} + d_2^2 M_{2k} M_{2h} + d_3^2 M_{3k} M_{3h}$. By

time-averaging equation 4, an expression for the mean effective cooling velocity is obtained

$$\bar{q}_e = G_{hk} \left(\bar{u}_h \bar{u}_k + \varepsilon^2 \overline{u'_h u'_k} \right) \quad (5)$$

where $\overline{u'_h u'_k}$ denotes the Reynolds stress tensor. An equation for the stochastic effective cooling velocity, q'_e , can be obtained by subtracting equation 5 from equation 4

$$\frac{q'_e}{\varepsilon} = G_{hk} \left(\bar{u}_h u'_k + \bar{u}_k u'_h + \varepsilon u'_h u'_k - \varepsilon \overline{u'_h u'_k} \right) \quad (6)$$

Squaring and averaging equation 6 yields

$$\frac{\overline{q_e'^2}}{\varepsilon^2} = G_{hk} G_{hk} \left(\overline{u_h^2 u'_k u'_k} + \overline{u_k^2 u'_h u'_h} + 2 \overline{u_h u_k u'_k u'_h} \right) + R \quad (7)$$

where R is a term that contains moments of the velocity fluctuations of third order or higher. Furthermore, if measurements are taken simultaneously with two probes, at two different locations, their signals are related to the velocity statistics by the relation

$$\frac{\overline{q_{e,a}' q_{e,b}'}}{\varepsilon^2} = G_{hk,a} G_{hk,b} \left(\overline{u_{h,a} u_{h,b} u'_{k,a} u'_{k,b}} + \overline{u_{k,a} u_{k,b} u'_{h,a} u'_{h,b}} + 2 \overline{u_{h,a} u_{k,b} u'_{k,a} u'_{h,b}} \right) + R \quad (8)$$

where subscripts a and b denote two separated points in space.

If m measurements are taken for different values of θ , then a set of simultaneous equations based on the time-averaged sensor response can be formed. For example, details of the mean flow field (to leading order) can be recovered by arranging equation 5 as a system of the form

$$\underbrace{\begin{bmatrix} G_{11}(\theta_1) & G_{22}(\theta_1) & G_{12}(\theta_1) \\ G_{11}(\theta_2) & G_{22}(\theta_2) & G_{12}(\theta_2) \\ \vdots & \vdots & \vdots \\ G_{11}(\theta_m) & G_{22}(\theta_m) & G_{12}(\theta_m) \end{bmatrix}}_{\mathbf{A}} \underbrace{\begin{bmatrix} \bar{u}_1 \bar{u}_1 \\ \bar{u}_2 \bar{u}_2 \\ \bar{u}_1 \bar{u}_2 \end{bmatrix}}_{\mathbf{x}} = \underbrace{\begin{bmatrix} \bar{q}_e(\theta_1) \\ \bar{q}_e(\theta_2) \\ \vdots \\ \bar{q}_e(\theta_m) \end{bmatrix}}_{\mathbf{b}} \quad (9)$$

Following the QR-factorisation of the coefficient matrix, \mathbf{A} , the linear system of equations 9 is solved using a least-squares fitting procedure. Relative to matrix inversions of the normal equations, a least-squares fitting procedure can give a more precise fitting for data acquired using rotating wire techniques (Fujita & Kovaszny, 1968).

Experimental configuration

The current measurement campaign was conducted in a low-speed linear compressor cascade facility. Following an upstream 3:1 wind-tunnel contraction, the Reynolds number, based on inlet velocity, U_∞ , and blade chord, c , was held fixed at 7.5×10^5 . The inlet free stream Mach number and turbulence intensity were measured to be 0.23 and 1.5%, respectively.

The linear compressor cascade is comprised of seven controlled diffusion airfoils and has no tip gaps. This flow

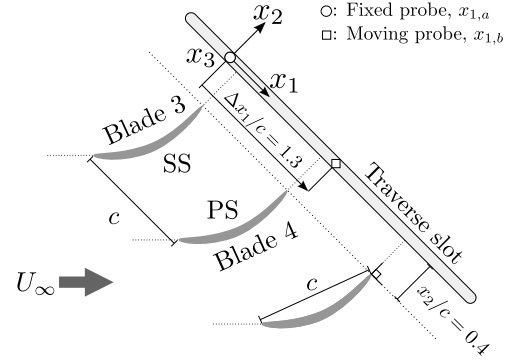


Figure 2. Schematic of the cascade central passages and inertial coordinate system, x_i . The position of the fixed (\circ) and moving (\square) probes are denoted $x_{1,a}$ and $x_{1,b}$, respectively. Note that the x_3 coordinate is measured in to the page.

configuration, therefore, is representative of a high-pressure stator row found in a modern turbofan engine. Each blade has unit aspect ratio, unit pitch-to-chord and a trailing edge thickness of $d/c = 0.05$. The central passages of the cascade are illustrated in Figure 2.

A pair of straight single-wire sensors were used over the course of the experimental campaign. Each sensor has a platinum-plated tungsten element aligned perpendicularly to the probe axis with a wire aspect ratio of 250.

Data acquisition and post-processing

The two probes were inserted through a traverse slot that lies parallel to the tangential x_1 axis, located an axial distance $x_2/c = 0.4$ downstream from the blade row trailing edge (see figure 2). Both sensors were held fixed at the mid-span position $x_3/c = 0.5$.

The origin of the inertial coordinate system, x_i , is defined by the position of the fixed sensor, which is located on the wake pressure side (PS) of blade 3. The tangential separation between the position of the fixed probe, $x_{1,a}$, and the position of the moving probe, $x_{1,b}$, is defined here as

$$\Delta x_1 \equiv x_{1,b} - x_{1,a}$$

Each line traverse starts with the two probes positioned at a minimum separation of $\Delta x_1/c = 0.01$, followed by consecutive measurements with a uniform spacing of $\Delta x_1/c = 0.025$. The line traverse finishes at a maximum separation of $\Delta x_1/c = 1.3$, as illustrated in figure 2. For every measurement point, both probes were rotated in phase from 0 to π in 10 equal increments.

Data was acquired for a sampling period of $t_s U_\infty/c \approx 4 \times 10^4$ at a sampling frequency of $f_s c/U_\infty = 100$, for both sensors at their respective measurement stations. Temperature variations were monitored by logging the output from a digital thermocouple, where a maximum drift of no more than $\pm 1^\circ\text{C}$ was observed. At the beginning and end of each traverse, both sensors were calibrated *in-situ* against a Pitot tube in a region of low turbulence intensity flow. The square of the mean wire voltage, \bar{E}^2 , was correlated to the mean ef-

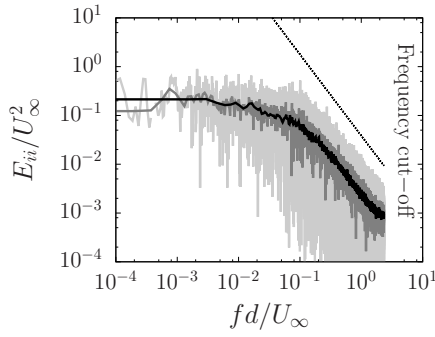


Figure 3. PSD estimation via Bartlett's method using $n/N = \{1 (\text{---}), 8 (\text{---}), 64 (\text{---})\}$ ensemble-averaged sub-series. The $-5/3$ law ($---$) is also plotted. All data has been normalised using the blade trailing edge thickness d and the inlet velocity U_∞ .

effective cooling velocity using King's Law

$$\bar{E}^2 = A + B\bar{q}_e^n \quad (10)$$

where the exponent n was prescribed a constant value of 0.45 and the coefficients A and B were determined using simple linear regression.

Over the course of the measurement campaign, a significant volume of binary data was accumulated. In order to post-process the raw data efficiently, certain CPU intensive tasks were executed on general purpose graphics processing units (GPGPU). For example, the Fourier decomposition of the stochastic effective cooling velocity required to estimate the power spectral density (PSD) was computed using GPGPU Fast Fourier Transform libraries¹.

The turbulence energy spectra can be computed by first noting that the PSD, E_{ii} , and the autocorrelation function, R_{ii} , form a Fourier transform pair

$$E_{ii}(f) \equiv \int_{-\infty}^{\infty} R_{ii}(\Delta t) e^{-j2\pi f \Delta t} d\Delta t \quad (11)$$

where f denotes frequency, Δt denotes temporal separation and j denotes the unit complex number. By ensemble-averaging the PSD computed from non-overlapping sub-series of the total time series, the variance of the spectra can be reduced by a factor of $\sqrt{(n/N)}$, where n is a sub-multiple of the total number of samples $N = f_{st_s}$ (Bartlett, 1948). Prior to computing the mean-squared amplitude of the Fourier coefficients, each sub-series of data was windowed using a Hann function. The PSD computed using $n/N = \{1, 8, 64\}$ ensemble-averaged sub-series is shown in Figure 3 and implies that the current measurements resolve eddies in both the energy-containing range and inertial sub-range.

RESULTS

This section reports turbulence statistics in the near-wake region of the cascade acquired using the methodology discussed in the previous section. The turbulent fluid

motions are characterised using both single- and two-point statistics and include details of Reynolds stresses, energy spectra, and space-time correlations.

Single-point measurements

In order to emphasise the relative positions of the suction side (SS) of blade 3 and pressure side (PS) of blade 4 to the centre of the wake (see figure 2), single-point measurements are plotted against the translated coordinate $\hat{x}_1 = x_1 - h$, where h denotes the position of the maximum mean axial velocity deficit. This convention is illustrated in figure 4, where the mean axial velocity profile normalised by the inlet velocity U_∞ is plotted.

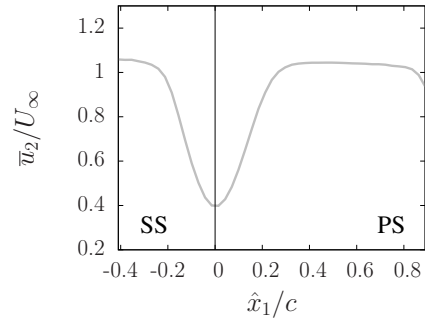


Figure 4. Profile of mean axial velocity, \bar{u}_2 . All data has been normalised using the blade chord c and the inlet velocity U_∞ .

Profiles of tangential and axial Reynolds stress normalised by the inlet velocity are plotted in Figure 5. On the wake SS ($\hat{x}_2 < 0$), the axial Reynolds stress dominates whereas, on the wake PS ($\hat{x}_2 > 0$), the two components have a similar magnitude. Comparable asymmetry between

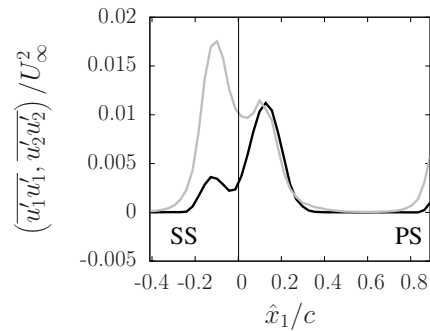


Figure 5. Reynolds stress profiles including tangential $\overline{u_1' u_1'}$ (---) and axial $\overline{u_2' u_2'}$ (---) components. All data has been normalised by blade chord c and the inlet velocity U_∞ .

turbulent stresses has also been observed in the near-wake region of compressor rotor blades (Ravindranath & Lakshminarayana, 1981) and originates from the differing turbulence properties on the blade SS and PS. Next, frequency-domain statistics are examined in order to clarify the disparity in Reynolds stresses on the wake SS.

¹NVIDIA CUDA Fast Fourier Transform library (cuFFT).

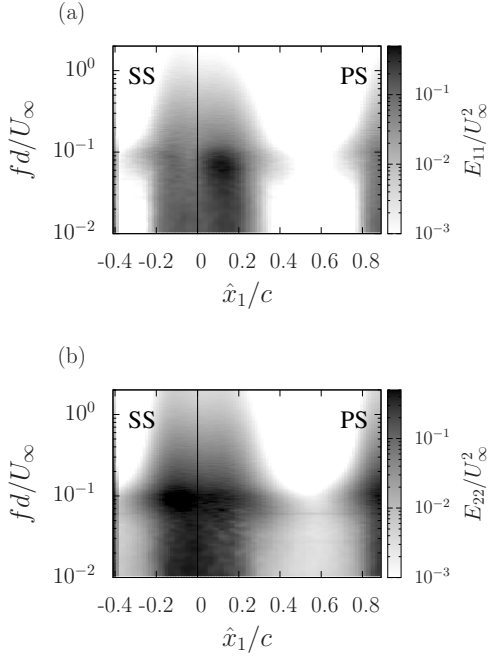


Figure 6. Contours of PSD including the (a) tangential E_{11} and (b) axial E_{22} components. All data has been normalised using the blade trailing edge thickness d and inlet velocity U_∞ .

Contours of tangential and axial PSD normalised by the inlet velocity are shown in figure 6. The dark patches across the wake SS and PS indicate that the regions of high turbulence energy are confined to reduced frequencies of less than 0.2. The most vigorous turbulence activity occurs at a reduced frequency of approximately 0.1 and coincides with the tangential position of peak axial Reynolds stress (see figure 5). This region can be interpreted as the spectral footprint of an upstream von Kármán vortex street shedding from the blade trailing edge. The integrated effect of this low-frequency high-energy motion is manifest as a strong axial turbulence intensity on the wake SS.

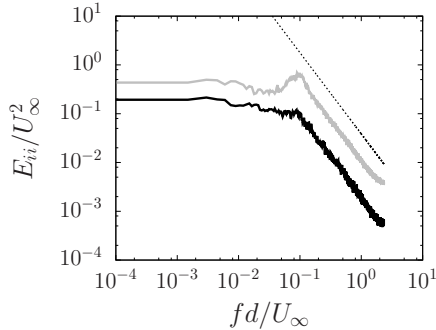


Figure 7. Line spectra of tangential, E_{11} (—), and axial, E_{22} (—), velocity components on the wake SS $\hat{x}_1/c = -0.12$. The $-5/3$ law (---) is also included. All data has been normalised using the blade trailing edge thickness d and the inlet velocity U_∞ .

Tangential and axial line spectra acquired on the wake SS ($\hat{x}_1/c = -0.12$) are plotted in Figure 7. As previously mentioned, the majority of turbulence energy on the wake SS is due to trailing edge vortices shedding at a reduced frequency of approximately 0.1. At higher frequencies, the turbulence energy spectrum decays in accordance with Kolmogorov's $-5/3$ Law and infers that the smaller scales retain their isotropy.

The autocorrelation coefficient functions for the tangential and axial velocity fluctuations are shown in Figure 8 and respectively resemble 'longitudinal' and 'transversal' correlations encountered in, for example, the wake of a circular cylinder (Grant, 1958). The differing correlation shapes on the wake SS infer that the turbulence in this region is far from disorganised (i.e. isotropic) and a well-defined structure is present. By invoking Taylor's frozen turbulence hypothesis, and assuming that the axial fluctuations convect at their local mean velocity, an integral length scale of approximately a quarter chord is obtained.

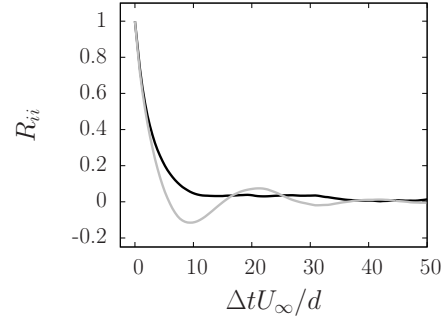


Figure 8. Autocorrelation coefficient function for tangential R_{11} (—) and axial R_{22} (—) velocity fluctuations. All data has been normalised using the blade trailing edge thickness d and inlet velocity U_∞ .

Two-point measurements

For the double anemometer configuration, the space-time correlation function for axial fluctuations, R_{22} , can be written as

$$R_{22}(\Delta x_1, \Delta t) = \frac{u'_2(x_{1,a}, t) u'_2(x_{1,b}, t + \Delta t)}{\sqrt{u'^2_2(x_{1,a}, t)} \sqrt{u'^2_2(x_{1,b}, t + \Delta t)}} \quad (12)$$

By regarding an eddy as a region of correlated turbulence, and assuming $R_{22} \rightarrow 0$ as $\Delta x_1 \rightarrow \infty$ and $\Delta t \rightarrow \infty$, equation 12 can be used to quantify the largest, most energetic motions present in the near-wake region (Grant, 1958).

The axial space-time correlation function is plotted in Figure 9. By assuming that temporal separation, $\Delta t U_\infty / c$, represents axial spatial separation, a two-dimensional picture of turbulence structure in the near-wake region is obtained. The axial velocity fluctuations remain correlated for up to twenty percent chord in both the tangential and axial directions, indicating that the eddies in this region have an isotropic structure on the x_{12} plane. In addition, vertical sections of R_{22} for $\Delta x_1/c < 0.25$ bear resemblance to

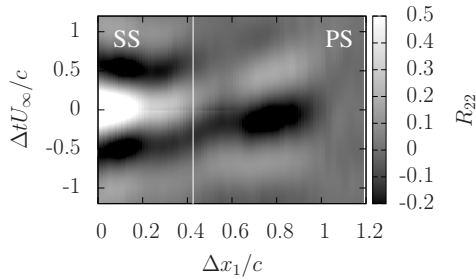


Figure 9. Space-time axial velocity correlation function, $R_{22}(\Delta x_2, \Delta t)$. Note that the correlation coefficient has been to clipped $R_{22} \in [-0.2, +0.5]$. All data has been scaled using the blade chord c and inlet velocity U_∞ .

the ‘transversal double velocity correlation’ in the turbulent wake of a cylinder (Townsend, 1976) and hint at a similar quasiperiodic structure in the near-wake region. Finally, the turbulent fluid motions remain correlated at tangential separations up to $\Delta x_1/c \approx 0.8$ which infer that structures approaching the size of the blade passage exist in the near-wake region.

SUMMARY AND FUTURE WORK

Single- and two-point hot-wire measurements were acquired in the wake of a linear compressor cascade at a chord Reynolds number of 7.5×10^5 using an experimental procedure based on a pair of rotated single straight-wire sensors. The current results infer an orderly turbulence structure in the near-wake region and, in particular, underline the existence of large-scale, energy-bearing eddies in compressor blade passages.

Future work will include a full area traverse on the x_{13} plane in order to clarify changes in turbulence structure as the end-wall region is approached. In addition, generalised hot-wire response equations will be derived in order to resolve all components of the Reynolds stress tensor. Finally, a detailed evaluation of the two-point correlation function could help develop a reduced-order model of turbulence structure in compressor blade passages that would prove useful to the modelling community.

ACKNOWLEDGEMENTS

The authors would like to thank Rolls-Royce plc and Innovate UK for their support of this work as part of the TuFT (Turbo-machinery Flow and Turbulence) project. T.J. would like to thank Henry Ng for the hot-wire diagrams.

REFERENCES

Adkins, G. G. & Smith, L. H. 1982 Spanwise Mixing in Axial Flow Turbomachines. *J. Eng. Gas Turbines Power* **104**, 97–110.

Bartlett, M. S. 1948 Smoothing Periodograms from Time-Series with Continuous Spectra. *Nature* **161**, 686–687.

Bissonnette, L. R. & Mellor, G. L. 1974 Experiments on the behaviour of an axisymmetric turbulent boundary layer with a sudden circumferential strain. *J. Fluid Mech.* **63**, 369–413.

Brundrett, E. & Baines, W. D. 1964 The production and diffusion of vorticity in duct flow. *J. Fluid Mech.* **19**, 375–394.

Bruun, H. H. 1995 *Hot-Wire Anemometry*, First edn. Oxford: Oxford University Press.

Camp, T. R. & Shin, H. W. 1995 Turbulence Intensity and Length Scale Measurements in Multistage Compressors. *Journal of Turbomachinery* **86**, 38–46.

Champagne, F. H. & Sleicher, C. A. 1967 Turbulence measurements with inclined hot-wires. Part 2. Hot-wire response equations. *J. Fluid Mech.* **28**, 177–182.

Cumpsty, N. A. 1989 *Compressor Aerodynamics*. Malabar, Florida: Krieger Publishing Company.

De Grande, G. & Kool, P. 1981 An improved experimental method to determine the complete Reynolds stress tensor with a single rotating hot wire. *J. Phys. E: Sci. Instrum.* **14**, 196–201.

Denton, J. D. 2010 Some limitations of turbomachinery CFD. *ASME Turbo Expo 2010; Power for Land, Sea, and Air; GT2010-22540*.

di Mare, L., Klein, M., Jones, W. P. & Janicka, J. 2006 Synthetic turbulence inflow conditions for large-eddy simulation. *Phys. Fluids* **18**, 025107.

Evans, R. L. 1975 Turbulence and Unsteadiness Measurements Downstream of a Moving Blade Row. *J. Eng. Gas Turbines Power* **97**, 131–137.

Fujita, H. & Kovaszny, L. S. G. 1968 Measurement of Reynolds Stress by a Single Rotated Hot Wire Anemometer. *Phys. Fluids* **39**, 1351–1355.

Gallimore, S. J. & Cumpsty, N. A. 1986 Spanwise Mixing in Multi-Stage Axial Flow Compressors Part I. Experimental Investigation. *Journal of Turbomachinery — Transactions of the ASME* **108**, 2–9.

Grant, H. L. 1958 The large eddies of turbulent motion. *J. Fluid Mech.* pp. 149–190.

Jørgensen, F. E. 1971 Directional sensitivity of wire and fibre-film probes. *DISA information no. 11*.

Lakshminarayana, B. & Reynolds, B. 1980 Turbulence Characteristics in the Near Wake of a Compressor Rotor Blade. *AIAA Journal* **18**, 1354–1362.

Muthanna, C. & Devenport, W. J. 2004 Wake of a Compressor Cascade with Tip Gap, Part 1: Mean Flow and Turbulence Structure. *AIAA Journal* **42**, 2320–2331.

Paulsen, L. 1983 Triple hot-wire technique for simultaneous measurements of instantaneous velocity components in turbulent flows. *J. Phys. E: Sci. Instrum.* **16**, 554–562.

Ravindranath, A. & Lakshminarayana, B. 1981 Structure and Decay Characteristics of Turbulence in the Near and Far-Wake of a Moderately Loaded Compressor Rotor-Blade. *Journal of Engineering and Power* **102**, 131–140.

Russ, S. & Simon, T. W. 1991 On the rotating, slanted, hot-wire technique. *Experiments in Fluids* **12**, 76–80.

Tian, Q., Lowe, K. T. & Simpson, R. L. 2007 A three-component laser-Doppler velocimeter for measurements inside the linear compressor cascade. *Exp. Fluids* **43**, 487–499.

Townsend, A. A. 1976 *The structure of turbulent shear flow*, Second edn. New York: Cambridge University Press.

Webster, C. A. G. 1962 A note on the sensitivity to yaw of a hot-wire anemometer. *J. Fluid Mech.* **20**, 307–312.

Wenger, C. W., Devenport, W. J., Wittmer, K. S. & Muthanna, C. 2004 Wake of a Compressor Cascade with Tip Gap, Part 3: Two-Point Statistics. *AIAA Journal* **42**, 2341–2346.